High-resolution infrared emission spectrum of InF

T. KARKANIS, M. DULICK, Z. MORBI, J.B. WHITE, AND P.F. BERNATH[1]
Centre for Molecular Beams and Laser Chemistry, Department of Chemistry, University of Waterloo, Waterloo, ON N2L 3G1, Canada

Received March 15, 1994
Accepted June 6, 1994

This paper is dedicated to Dr. Gerhard Herzberg on the occasion of his 90th birthday

A high-resolution infrared emission spectrum of InF was recorded with a Fourier transform spectrometer. A total of 2664 rotational lines from $v = 1 \rightarrow 0$ to $v = 12 \rightarrow 11$ were measured for the major isotopomer ^{115}InF and 179 lines for $v = 1 \rightarrow 0$ and $v = 2 \rightarrow 1$ for the minor isotope ^{113}InF in the $X^1\Sigma^+$ ground state. Revised Dunham Y_{ij} constants for each isotopomer as well as isotopically invariant Dunham U_{ij} constants are reported. Also, an effective Born–Oppenheimer potential was determined by fitting the data directly to the eigenvalues of a parameterized potential.

Un spectre d'émission infrarouge de InF à haute résolution a été obtenu avec un spectromètre à transformée de Fourier. On a mesuré au total 2664 raies de rotation de $v = 1 \rightarrow 0$ à $v = 12 \rightarrow 11$ pour le principal isopotomère ^{115}InF et 179 raies de $v = 1 \rightarrow 0$ et $v = 2 \rightarrow 1$ pour la variété moins abondante ^{113}InF, dans l'état fondamental $X^1\Sigma^+$. Des valeurs révisées sont présentées pour les constantes Y_{ij} de Dunham, ainsi que pour les constantes de Dunham isotopiquement invariantes U_{ij}. On a aussi déterminé un potentiel Born–Oppenheimer effectif en ajustant directement les données aux valeurs propres d'un potentiel paramétrisé.

[Traduit par la rédaction]

Can. J. Phys. 72, 1213 (1994)

1. Introduction

The first comprehensive spectroscopic study of InF was conducted by Barrow and co-workers [1–3] in the early 1950s. They were able to identify three prominent electronic transitions in their UV absorption and emission spectra, $A^3\Pi_0$–$X^1\Sigma^+$, $B^3\Pi_1$–$X^1\Sigma^+$, and $C^1\Pi$–$X^1\Sigma^+$, and confirmed the electronic assignments for A–X and B–X through a rotational analysis of selected bands. In a more recent study, Nampoori et al. [4] were successful in finally resolving and analyzing the rotational structure in a number of C–X bands, thereby confirming the C–X electronic assignments of Barrow.

During the past few decades the majority of investigations concentrated on the analysis of InF in the microwave and infrared regions of the spectrum. Lovas and Törring [5] analyzed the hyperfine structure (hfs) in the $v = 0$ and 1 vibrational levels of ^{115}InF $X^1\Sigma^+$ from the $J = 1 \rightarrow 2$ and $J = 2 \rightarrow 3$ microwave transitions. The subsequent studies by Hoeft et al. [6] extended the previous hfs analysis by recording $J = 0 \rightarrow 1$, $J = 16 \rightarrow 17$, $J = 17 \rightarrow 18$, and $J = 18 \rightarrow 19$ transitions for the first few vibrational levels of ^{115}InF, and $J = 0 \rightarrow 1$, $J = 16 \rightarrow 17$, and $J = 17 \rightarrow 18$ for $v = 0$ of ^{113}InF. The radiofrequency molecular beam resonance experiments by Hammerle et al. [7] lead to a further refinement of the quadrupole hfs constants for the lower v, J levels as well as establishing an upper limit for the hexadecapole hfs constant.

In the infrared region Uehara et al. [8] first recorded a 0.1 cm^{-1} low-resolution Fourier transform (FT) emission spectrum of ^{115}InF bands up to $v = 6$. This work was then superseded by the high resolution diode laser measurements of Ozaki et al. [9] that encompassed rovibrational transitions up to $v = 9$ for ^{115}InF and $v = 4$ for ^{113}InF.

In this paper we report on the analysis of the high-resolution Fourier transform infrared emission spectrum of InF. The continuous wave-number coverage of our FT spectrum has enabled us to fill in many of the gaps in the tables of the measured line positions given in ref. 9. In addition we also report revised values of Dunham Y's and isotopically invariant Dunham U's, including a parameterized Born–Oppenheimer potential, which were derived from fits of a data set that combined our measured line positions with microwave rotational line centers and ^{113}InF isotopomer data from ref. 9.

2. Experimental details

A high-resolution emission spectrum of InF was recorded over the wave-number range 360–760 cm^{-1} with a Bruker IFS 120 HR spectrometer. Gas-phase InF was produced by reacting indium metal vapor with SF_6 over the temperature range of 1200–1500°C in a 1.2 m mullite tube with KRS-5 windows. An interferogram was recorded by coadding 20 individual scans at a resolution of 0.006 cm^{-1} with a liquid helium-cooled Si:B detector and a 3.5 μm Mylar beamsplitter. The interferogram was then transformed to obtain the frequency spectrum that was used in the measurement of line positions. A portion of the spectrum in the vicinity of the (1, 0) R-branch band head is displayed in Fig. 1.

Rotational line frequencies were determined using Brault's computer program PC-DECOMP. A total of 2840 lines were measured with 2664 lines from the major isotopomer ^{115}InF (95% abundance) and 179 from the minor isotopomer ^{113}InF (5% abundance). Resolved ^{115}InF lines were observed in both the P and R branches of the (1, 0) through (12, 11) bands while spectral congestion limited the observation of resolved ^{113}InF lines to only the R branches of the (1, 0) and (2, 1) bands. The complete list of measured line positions is given in Table 1.[2]

The measured InF rotational lines were then calibrated with respect to HF emission lines also present in the spectrum [10]. Intense and unblended lines with a signal-to-noise ratio of ≈25 were measured to a precision of ±0.0001 cm^{-1}. Typically,

[1] Author to whom correspondence may be addressed.

[2] Due to space limitations Table 1 cannot be reproduced here. Copies of this table on deposit may be purchased from: The Depository of Unpublished Data, Document Delivery, CISTI, National Research Council Canada, Ottawa, ON K1A 0S2, Canada.

Printed in Canada / Imprimé au Canada

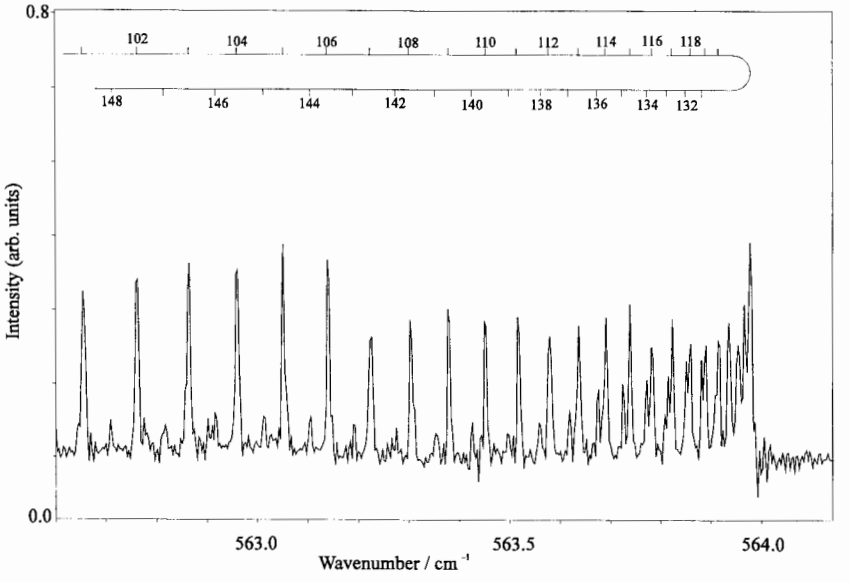

FIG. 1. Portion of the InF infrared emission spectrum in the vicinity of the ^{115}InF (1, 0) R-branch band head.

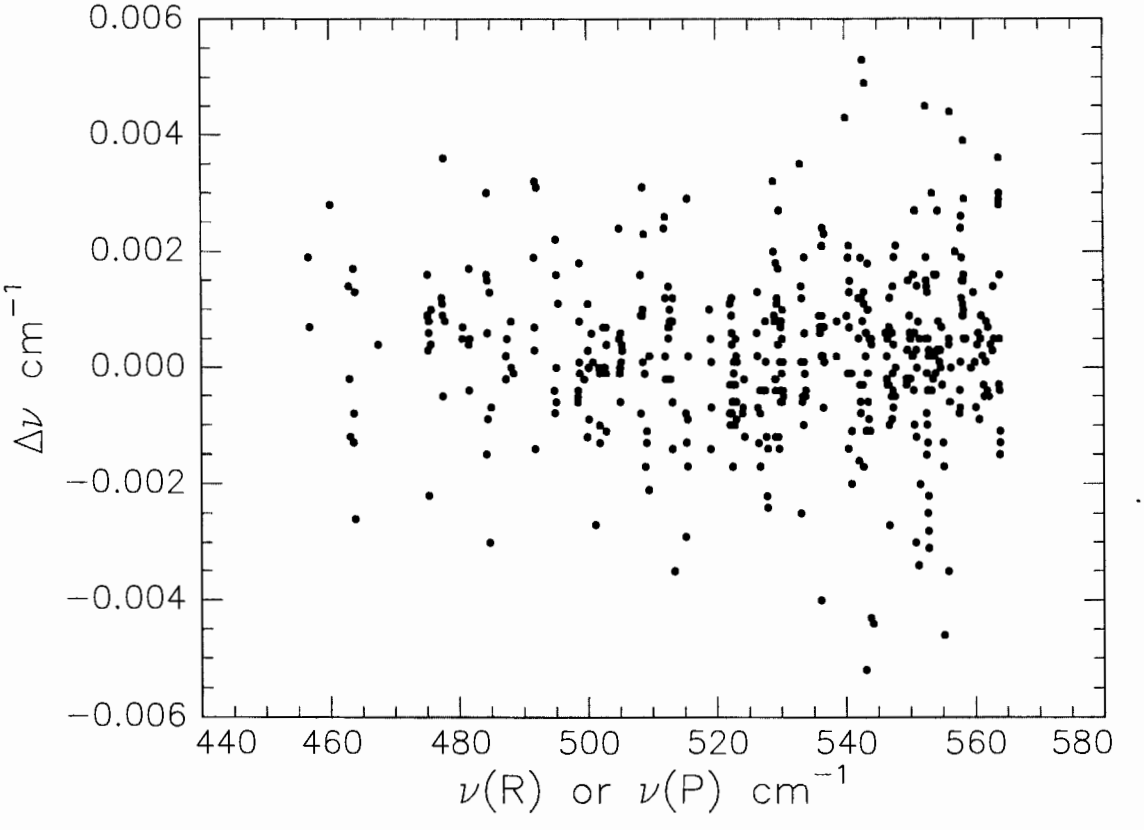

FIG. 2. A scatter plot that compares the ref. 9 ^{115}InF line frequencies relative to ours ($\Delta\nu$) plotted as a function of our measured line frequencies ($\nu(R)$ or $\nu(P)$).

however, weak and blended lines, which constituted the vast majority of lines in the data set, were measured at best to a precision of ± 0.0008 cm^{-1}. The above stated precisions are based solely on the internal consistency obtained when calibration was done on a selected group of lines using all the available sharp and intense HF lines in the recorded spectrum.

To obtain an independent confirmation of our accuracy, a comparison was made between ^{115}InF lines common to our data set and those from ref. 9. The results from this comparison are summarized in Fig. 2. A simple statistical analysis of these differences yielded a mean of 0.0002 cm^{-1} and ± 0.0014 cm^{-1} for the 1σ rms deviation. The fact that the differences are randomly distributed about a mean of 0.0002 cm^{-1} (statistically insignificant from zero) indicates the absence of any serious systematic shifts in the measurement or calibration of either data set. However, the crucial result, the estimated error reported in

TABLE 2. Isotopically dependent Dunham constants in cm^{-1}

		^{115}InF	^{113}InF
	Y_{10}	535.363 34 (12)	536.034 89 (56)
	Y_{20}	−2.672 556 (37)	−2.678 74 (24)
10^3	Y_{30}	8.472 6 (41)	8.324 (32)
10^5	Y_{40}	−1.741 (15)	
	Y_{01}	0.262 323 787 (32)	0.262 982 99 (12)
10^3	Y_{11}	−1.879 650 (18)	−1.886 93 (16)
10^6	Y_{21}	4.936 4 (37)	5.044 (18)
10^9	Y_{31}	1.67 (16)	
10^7	Y_{02}	−2.518 51 (19)	−2.529 1 (22)
10^{11}	Y_{12}	6.01 (20)	7.8 (21)
10^{12}	Y_{22}	8.53 (14)	
10^{13}	Y_{03}	−1.115 2 (78)	−1.19 (28)
10^{16}	Y_{13}	9.60 (71)	

TABLE 3. Isotopically invariant Dunham constants in cm^{-1}

		Unconstrained	Constrained
	U_{10}	2161.625 71 (46)	2161.625 42 (44)
	U_{20}	−43.570 16 (58)	−43.569 99 (56)
	U_{30}	0.557 66 (26)	0.557 69 (26)
10^3	U_{40}	−4.621 (40)	−4.641 (40)
	U_{01}	4.276 628 18 (32)	4.276 629 69 (18)
	U_{11}	−0.123 729 49 (84)	−0.123 730 59 (57)
10^3	U_{21}	1.312 09 (90)	1.310 54 (60)
10^6	U_{31}	1.78 (16)	2.39 (16)
10^5	U_{02}	−6.693 86 (48)	−6.695 82
10^8	U_{12}	6.46 (17)	6.954 59
10^8	U_{22}	3.689 (53)	3.801 05
10^{10}	U_{32}		−6.961 41
10^{10}	U_{03}	−4.828 (33)	−4.584 08
10^{11}	U_{13}	1.68 (11)	1.375 35
10^{14}	U_{23}		1.485 89
10^{14}	U_{04}		−1.101 95
10^{16}	U_{14}		6.333 34
10^{17}	U_{24}		2.323 41
10^{19}	U_{05}		−2.288 45
10^{21}	U_{15}		6.992 42
10^{24}	U_{06}		−4.765 53
10^{25}	U_{16}		8.006 80
10^{28}	U_{07}		−1.235 21
10^{33}	U_{08}		−2.052 50

ref. 9, ≤ 0.002 cm^{-1}, vs. the rms deviation of 0.0014 cm^{-1} for the differences, indicates at least by this simple analysis that the rms error in our measurements is ≤ 0.0005 cm^{-1}.

3. Results and discussion

Two types of Dunham constants, the isotopically dependent Y_{ij}'s and the isotopically invariant U_{ij}'s, are listed in Tables 2 and 3, respectively. The Y_{ij}'s for each isotopomer were determined by separately fitting the rotational lines of each isotopomer to the conventional Dunham energy level expression [11]

$$E(v, J) = \sum_{i,j} Y_{ij} \left(v + \frac{1}{2} \right)^i [J(J+1)]^j \qquad (1)$$

while the U_{ij}'s were determined by fitting the combined set of isotopomer lines to [12, 13]

$$E(v, J) = \sum_{i,j} \mu^{-(i+2j)/2} U_{ij} \left(1 + \frac{m_e}{M_A} \Delta_{ij}^A + \frac{m_e}{M_B} \Delta_{ij}^B \right) \times \left(v + \frac{1}{2} \right)^i [J(J+1)]^j \qquad (2)$$

where μ is reduced mass, m_e is electron mass, M_A and M_B are atomic masses for centers A and B, and Δ_{ij}^A and Δ_{ij}^B are Born–Oppenheimer breakdown parameters. Because naturally occurring fluorine is 100% ^{19}F, all isotopic information on Born–Oppenheimer breakdown is conveyed only by the indium center and hence only Δ_{ij}'s for the indium center are determinable from a least-squares fit of the data. The designation "unconstrained" in Table 3 refers to the fit where all U_{ij}'s were treated as adjustable parameters while "constrained" refers to the fit where only the $j = 0$ and 1 U_{ij}'s were adjusted, with all remaining U_{ij}'s fixed to values determined from the constrained U relations of the Dunham model [14].

The standard deviations for the ^{115}InF and ^{113}InF Dunham Y fits were 0.866 and 0.653, respectively. In the case of the isotopically invariant Dunham U fits, the standard deviations were 0.851 for the unconstrained fit and 0.859 for the constrained fit. However, the unconstrained fit involved a total of 13 adjustable parameters while the constrained fit yielded essentially the same standard deviation with only 8 adjustable parameters. On this basis the constrained fit is deemed the superior fit and it is for this reason we report only the residuals obtained from the constrained fit in Table 1.

Because of indium's large atomic mass one would expect, from (2), the Born–Oppenheimer breakdown to be an imperceptible effect on the rovibrational levels of InF. But results from a preliminary constrained fit seemed to indicate otherwise, with a value of $\Delta_{10} = -5.72 \pm 1.67$ determined to slightly better than 3 standard deviations. However, we dismissed this result and decided to fix Δ_{10} to zero in the final fit based on the following considerations. Treating Δ_{10} as an adjustable parameter vs. fixing it to zero leads to only a 0.1% improvement in the standard deviation of the fit. Large statistical correlation between Δ_{10} and U_{10} most likely means that the uncertainity in Δ_{10} is an unreliable statistic. The limited number of ^{113}InF IR lines (involving only the first few vibrational levels) and three microwave rotational lines makes the determination of Δ_{10} seem even less plausible. Most important of all is the confirmation obtained from an independent fit of the data to the eigenvalues of a parameterized potential (discussed below), which indicated the total absence of Born–Oppenheimer breakdown.

Finally, two additional points must be made in regard to these Dunham fits. As was stated in the previous section, only resolved R lines were observed for the minor isotopomer ^{113}InF. To obtain a reasonably good Y fit for ^{113}InF the inclusion of ^{113}InF P lines from ref. 9 was required. This was necessary to prevent distortion in the values of the ^{113}InF Y_{ij}'s that results from exclusively fitting $\Delta J = +1$ rotational transitions. In other words, we achieved better estimates for the Y's by "balancing" the fit with $\Delta J = +1$ and -1 transitions to reduce statistical correlation.

The lines in Table 1 were also used to determine an effective Born–Oppenheimer potential using a method[3] similiar to the one developed by Coxon and Hajigeorgiou [15, 16]. Briefly, the calculation entailed a fit of the data to the eigenvalues of the radial Schrödinger equation

TABLE 4. Equation (6) Born–Oppenheimer potential parameters

D_e (cm^{-1})	42 300.0
R_e (Å)	1.985 397 300 6 (214)
β_0	5.082 289 283 (117)
β_1	0.528 030 82 (235)
β_2	2.013 559 9 (691)
β_3	10.994 45 (153)
M_A (^{115}In)	114.903 882
M_A (^{113}In)	112.904 061
M_B (^{19}F)	18.998 403 22

$$\left\{\frac{\hbar^2}{2\mu}\nabla^2 - U^{\text{eff}}(R) + E(v,J) - \frac{\hbar^2}{2\mu}[1 + q(R)]\frac{J(J+1)}{R^2}\right\}\psi(r; v, J) = 0 \quad (3)$$

where the effective internuclear potential for vibrational motion is modeled as

$$U^{\text{eff}}(R) = U^{\text{BO}}(R) + \frac{U_A(R)}{M_A} + \frac{U_B(R)}{M_B} \quad (4)$$

and the form of the Born–Oppenheimer potential is chosen as

$$U^{\text{BO}} = \frac{D_e\{1 - \exp[-\beta(R)]\}^2}{\{1 - \exp[-\beta(\infty)]\}^2} \quad (5)$$

where

$$\beta(R) = z\sum_{i=0}\beta_i z^i \quad (6)$$

$$\beta(\infty) = \sum_{i=0}\beta_i \quad (7)$$

and

$$z = \frac{(R - R_e)}{(R + R_e)} \quad (8)$$

The two remaining terms in (4) are corrections for Born–Oppenheimer breakdown and homogeneous nonadiabatic mixing for atomic centers A and B and are represented by the power series expansions

$$U_A(R) = \sum_{i=1} u_i^A (R - R_e)^i \quad (9)$$

and

$$U_B(R) = \sum_{i=1} u_i^B (R - R_e)^i \quad (10)$$

Similarly, $q(R)$ takes into account J-dependent Born–Oppenheimer breakdown and heterogeneous nonadiabatic mixing and is also represented by a power series expansion of the form

[3] M. Dulick and P.F. Bernath, manuscript in preparation.

TABLE 5. Calculated Dunham potential constants derived from the β parameters listed in Table 4

a_0	273 148.705 0 (126)
a_1	−3.437 248 389 (414)
a_2	7.977 469 88 (498)
a_3	−14.843 201 (106)
a_4	23.124 547 (579)
a_5	−30.220 96 (195)
a_6	31.565 95 (502)
a_7	−20.924 9 (107)
a_8	−8.405 1 (197)
a_9	61.367 8 (317)
a_{10}	−138.108 2 (448)

$$q(R) = M_A^{-1}\sum_{i=0} q_i^A (R - R_e)^i + M_B^{-1}\sum_{i=0} q_i^B (R - R_e)^i \quad (11)$$

Results from the parameterized potential fit where the final standard deviation was 0.885 are summarized in Table 4. Listed uncertainties are quoted to a standard deviation of 1σ. The value of D_e used in the fit corresponds to the thermochemical value quoted in ref. 17 and the atomic masses were obtained from ref. 18. Numerical integration of the Schrödinger equation was performed over the range 1.0 Å ≤ R ≤ 3.5 Å, with a grid spacing of 0.0025 Å (1Å = 10^{-10} m). And finally, as mentioned above, the fit was unable to determine any of the Born–Oppenheimer parameters appearing in (9)–(11).

In addition to reporting β's that correspond to our parameterized form of the Born–Oppenheimer potential given by (5), we also list in Table 5 Dunham potential constants that were generated by equating each term in the Dunham expansion to the corresponding term in the power series expansion of $U^{\text{BO}}(R)$ given by (5). Explicit relations between the a's and β's as well as a description of the method used in estimating the uncertainties in the a's are given in ref. 19.

4. Conclusion

Three important advantages often cited for using the technique of detecting infrared emission with a FT spectrometer are the unique capability of combining high resolution with wide and continuous spectral coverage, superior contrast between signal and background, and highly accurate measurements of line positions. In the infrared spectra of diatomic metal halides, especially those that contain a heavy metal or halide atom, spectral congestion poses a major obstacle toward resolving the fine structure. In this regard one often wonders whether the FT spectrometer is even capable of sufficiently resolving such spectra in order to conduct a proper rotational analysis.

In this sense, analysis of the infrared emission spectrum of InF reported here serves as a test case. Spectral congestion limited the FT in most instances to partially resolving the rotational lines of overlapping bands in the spectrum. As a result, the overall accuracy of our measured line positions, 0.0008 cm^{-1}, represents only a marginal improvement over the ≤0.002 cm^{-1} accuracy of lines measured in the diode laser spectrum [9]. Nevertheless, a sufficient number of completely resolved lines (accuracy ~0.0001 cm^{-1}) were found (~1/3 of the 2840 lines measured), due in large part to the wide range of

$P(J)$ and $R(J)$ lines ($J > 100$) present in the spectrum. The smaller set of unblended lines together with the larger set of weak and blended lines were quite adequate to determine reasonably good estimates for the Dunham Y and U constants.

Admittedly, such a simple test conducted on a $^1\Sigma^+$ ground state does not guarantee that applying this technique to a more complex IR diatomic halide spectrum involving a $^{2S+1}\Lambda$ ($S > 0$ and $\Lambda > 0$) ground state will always be successful. The encouraging results from this study at the very least warrant further investigation.

Acknowledgements

This work was supported by the Natural Sciences and Engineering Research Council of Canada (NSERC). Acknowledgement is made to the Petroleum Research Fund, administered by the American Chemical Society, for partial support of this work. We also wish to thank J. Ogilvie for communicating the constrained Dunham U relations prior to publication.

1. D. Welti and R.F. Barrow. Nature, **168**, 161 (1951).
2. R.F. Barrow, J.A.T. Jacquest, and E.W. Thompson. Proc. Phys. Soc. London Sect. A, **67**, 528 (1954).
3. R.F. Barrow, D.V. Glaser, and P.B. Zeeman. Proc. Phys. Soc. London Sect. A, **68**, 962 (1955).
4. V.P.N. Nampoori, M.N. Kamalasanan, and M.M. Patel. J. Phys. B: At. Mol. Phys. **8**, 2841 (1975).
5. F.J. Lovas and T. Törring. Z. Naturforsch. **24A**, 634 (1969).
6. J. Hoeft, F.J. Lovas, E. Tiemann, and T. Törring. Z. Naturforsch. A: Astrophys. Phys. Phys. Chem. **25A**, 1029 (1970); J. Hoeft and K.P.R. Nair. Z. Phys. D: Part. Fields, **29**, 203 (1994).
7. R.H. Hammerle, R. Van Ausdal, and J.C. Zorn. J. Chem. Phys. **57**, 4068 (1972).
8. H. Uerhara, K. Horiai, T. Mitani, and H. Suguro. Chem. Phys. Lett. **162**, 137 (1989).
9. Y. Ozaki, K. Horiari, K. Nakagawa, and H. Uehara. J. Mol. Spectrosc. **158**, 363 (1993).
10. H.G. Hedderich, K. Walker, and P.F. Bernath. J. Mol. Spectrosc. **149**, 314 (1991); R.N. Le Blanc, J.B. White, and P.F. Bernath. J. Mol. Spectrosc. **164**, 574 (1994).
11. J.L. Dunham. Phys. Rev. **41**, 721 (1932).
12. A.H.M. Ross, R.S. Eng, and H. Kildal. Opt. Commun. **12**, 433 (1974).
13. J.K.G. Watson. J. Mol. Spectrosc. **80**, 411 (1980).
14. J. Ogilvie. Comput. Phys. Commun. **30**, 101 (1983).
15. J.A. Coxon and P.G. Hajigeorgiou. Can. J. Phys. **70**, 40 (1992).
16. J.A. Coxon and P.G. Hajigeorgiou. Chem. Phys. **167**, 327 (1992).
17. K.P. Huber and G. Herzberg. Constants of diatomic molecules. Van Nostrand–Reinhold, New York. 1979.
18. I. Mills, T. Cvitaš, K. Homann, N. Kallay, and K. Kuchitsu. Quantities, units, and symbols in physical chemistry. Blackwell. Oxford, U.K. 1989.
19. H.G. Hedderich, M. Dulick, and P.F. Bernath. J. Chem. Phys. **99**. 8363 (1993).